

Photon beam asymmetry  $\Sigma$  in the reaction  $\bar{\gamma}p \rightarrow p\omega$  for  $E_\gamma = 1.152$  to  $1.876$  GeV

P. Collins<sup>b,g</sup>, B.G. Ritchie<sup>b,\*</sup>, M. Dugger<sup>b</sup>, F.J. Klein<sup>g,r</sup>, A.V. Anisovich<sup>c</sup>, E. Klempt<sup>c,1</sup>, V.A. Nikonov<sup>c,p</sup>, A. Sarantsev<sup>c,p</sup>, K.P. Adhikari<sup>ac</sup>, S. Adhikari<sup>n</sup>, D. Adikaram<sup>ag,1</sup>, Z. Akbar<sup>o</sup>, S. Anefalos Pereira<sup>u</sup>, H. Avakian<sup>an</sup>, J. Ball<sup>h</sup>, N.A. Baltzell<sup>an,al</sup>, M. Bashkanov<sup>ap</sup>, M. Battaglieri<sup>v</sup>, V. Batourine<sup>an,ab</sup>, I. Bedlinskiy<sup>z</sup>, A.S. Biselli<sup>l,f</sup>, S. Boiarinov<sup>an</sup>, W.J. Briscoe<sup>r</sup>, W.K. Brooks<sup>ao</sup>, V.D. Burkert<sup>an</sup>, Frank Thanh Cao<sup>j</sup>, T. Cao<sup>al,2</sup>, D.S. Carman<sup>an</sup>, A. Celentano<sup>v</sup>, G. Charles<sup>ag</sup>, T. Chetry<sup>af</sup>, G. Ciullo<sup>t,m</sup>, L. Clark<sup>aq</sup>, P.L. Cole<sup>s</sup>, M. Contalbrigo<sup>t</sup>, O. Cortes<sup>s</sup>, V. Crede<sup>o</sup>, N. Dashyan<sup>au</sup>, R. De Vita<sup>v</sup>, E. De Sanctis<sup>u</sup>, M. Defurne<sup>h</sup>, A. Deur<sup>an</sup>, C. Djalali<sup>al</sup>, R. Dupre<sup>y</sup>, H. Egiyan<sup>an,ad</sup>, A. El Alaoui<sup>ao</sup>, L. El Fassi<sup>ac</sup>, P. Eugenio<sup>o</sup>, G. Fedotov<sup>al,ak</sup>, A. Filippi<sup>x</sup>, J.A. Fleming<sup>ap</sup>, Y. Ghandilyan<sup>au</sup>, G.P. Gilfoyle<sup>ai</sup>, K.L. Giovanetti<sup>aa</sup>, F.X. Girod<sup>an</sup>, D.I. Glazier<sup>aq</sup>, C. Gleason<sup>al</sup>, E. Golovatch<sup>ak</sup>, R.W. Gothe<sup>al</sup>, K.A. Griffioen<sup>at</sup>, M. Guidal<sup>y</sup>, K. Hafidi<sup>a</sup>, H. Hakobyan<sup>ao,au</sup>, C. Hanretty<sup>an</sup>, N. Harrison<sup>an</sup>, M. Hattawy<sup>a</sup>, D. Heddle<sup>i,an</sup>, K. Hicks<sup>af</sup>, G. Hollis<sup>al</sup>, M. Holtrop<sup>ad</sup>, S.M. Hughes<sup>ap</sup>, Y. Ilieva<sup>al,r</sup>, D.G. Ireland<sup>aq</sup>, B.S. Ishkhanov<sup>ak</sup>, E.L. Isupov<sup>ak</sup>, D. Jenkins<sup>ar</sup>, H. Jiang<sup>al</sup>, H.S. Jo<sup>y</sup>, S. Joosten<sup>am</sup>, D. Keller<sup>as</sup>, G. Khachatryan<sup>au</sup>, M. Khachatryan<sup>ag</sup>, M. Khandaker<sup>ae,3</sup>, A. Kim<sup>j</sup>, W. Kim<sup>ab</sup>, A. Klein<sup>ag</sup>, V. Kubarovsky<sup>an,ah</sup>, S.V. Kuleshov<sup>ao,z</sup>, L. Lanza<sup>w</sup>, P. Lenisa<sup>t</sup>, K. Livingston<sup>aq</sup>, I.J.D. MacGregor<sup>aq</sup>, N. Markov<sup>j</sup>, B. McKinnon<sup>aq</sup>, C.A. Meyer<sup>f</sup>, Z.E. Meziani<sup>am</sup>, T. Mineeva<sup>ao</sup>, V. Mokeev<sup>an,ak</sup>, R.A. Montgomery<sup>aq</sup>, A. Movsisyan<sup>t</sup>, E. Munevar<sup>an</sup>, C. Munoz Camacho<sup>y</sup>, P. Nadel-Turonski<sup>an,r</sup>, L.A. Net<sup>al</sup>, S. Niccolai<sup>y</sup>, G. Niculescu<sup>aa</sup>, I. Niculescu<sup>aa</sup>, M. Osipenko<sup>v</sup>, A.I. Ostrovidov<sup>o</sup>, M. Paolone<sup>am</sup>, R. Paremuzyan<sup>ad</sup>, K. Park<sup>an,ab</sup>, E. Pasyuk<sup>an,b</sup>, W. Phelps<sup>n</sup>, S. Pisano<sup>u</sup>, O. Pogorelko<sup>z</sup>, J.W. Price<sup>d</sup>, S. Procureur<sup>h</sup>, Y. Prok<sup>ag,as,an</sup>, D. Protopopescu<sup>aq</sup>, B.A. Raue<sup>n,an</sup>, M. Ripani<sup>v</sup>, A. Rizzo<sup>w,aj</sup>, G. Rosner<sup>aq</sup>, F. Sabatié<sup>h</sup>, C. Salgado<sup>ae</sup>, R.A. Schumacher<sup>f</sup>, Y.G. Sharabian<sup>an</sup>, A. Simonyan<sup>au</sup>, Iu. Skorodumina<sup>al,ak</sup>, G.D. Smith<sup>ap</sup>, D.I. Sober<sup>g</sup>, D. Sokhan<sup>aq</sup>, N. Sparveris<sup>am</sup>, I. Stankovic<sup>ap</sup>, S. Stepanyan<sup>an</sup>, I.I. Strakovsky<sup>r</sup>, S. Strauch<sup>al,r</sup>, M. Taiuti<sup>q,4</sup>, M. Ungaro<sup>an,j</sup>, H. Voskanyan<sup>au</sup>, E. Voutier<sup>y</sup>, N.K. Walford<sup>g</sup>, D.P. Watts<sup>ap</sup>, X. Wei<sup>an</sup>, M.H. Wood<sup>e,al</sup>, N. Zachariou<sup>ap</sup>, J. Zhang<sup>an,ag</sup>, Z.W. Zhao<sup>ag,k</sup>

<sup>a</sup>Argonne National Laboratory, Argonne, Illinois 60439

<sup>b</sup>Arizona State University, Tempe, Arizona 85287-1504

<sup>c</sup>Helmholtz-Institut für Strahlen- und Kernphysik, Universität Bonn, Germany

<sup>d</sup>California State University, Dominguez Hills, Carson, CA 90747

<sup>e</sup>Canisius College, Buffalo, NY

<sup>f</sup>Carnegie Mellon University, Pittsburgh, Pennsylvania 15213

<sup>g</sup>Catholic University of America, Washington, D.C. 20064

<sup>h</sup>Irfu/SPH, CEA, Université Paris-Saclay, 91191 Gif-sur-Yvette, France

<sup>i</sup>Christopher Newport University, Newport News, Virginia 23606

<sup>j</sup>University of Connecticut, Storrs, Connecticut 06269

<sup>k</sup>Duke University, Durham, North Carolina 27708-0305

<sup>l</sup>Fairfield University, Fairfield CT 06824

<sup>m</sup>Università di Ferrara, 44121 Ferrara, Italy

<sup>n</sup>Florida International University, Miami, Florida 33199

<sup>o</sup>Florida State University, Tallahassee, Florida 32306

<sup>p</sup>NRC "Kurchatov" Institute, PNPI, Gatchina 188300, Russia

<sup>q</sup>Università di Genova, 16146 Genova, Italy

<sup>r</sup>The George Washington University, Washington, DC 20052

<sup>s</sup>Idaho State University, Pocatello, Idaho 83209

<sup>t</sup>INFN, Sezione di Ferrara, 44100 Ferrara, Italy

<sup>u</sup>INFN, Laboratori Nazionali di Frascati, 00044 Frascati, Italy

<sup>v</sup>INFN, Sezione di Genova, 16146 Genova, Italy

<sup>w</sup>INFN, Sezione di Roma Tor Vergata, 00133 Rome, Italy

<sup>x</sup>INFN, Sezione di Torino, 10125 Torino, Italy

<sup>y</sup>Institut de Physique Nucléaire, CNRS/IN2P3 and Université Paris Sud, Orsay, France

<sup>z</sup>Institute of Theoretical and Experimental Physics, Moscow, 117259, Russia

<sup>aa</sup>James Madison University, Harrisonburg, Virginia 22807

<sup>ab</sup>Kyungpook National University, Daegu 41566, Republic of Korea

<sup>ac</sup>Mississippi State University, Mississippi State, MS 39762-5167

<sup>ad</sup>University of New Hampshire, Durham, New Hampshire 03824-3568

<sup>ae</sup>Norfolk State University, Norfolk, Virginia 23504

<sup>af</sup>Ohio University, Athens, Ohio 45701

<sup>ag</sup>Old Dominion University, Norfolk, Virginia 23529

\*Corresponding author

<sup>1</sup>Current address: Newport News, Virginia 23606

<sup>2</sup>Current address: Hampton, VA 23668

<sup>3</sup>Current address: Pocatello, Idaho 83209

<sup>4</sup>Current address: 16146 Genova, Italy

<sup>ah</sup>*Rensselaer Polytechnic Institute, Troy, New York 12180-3590*  
<sup>ai</sup>*University of Richmond, Richmond, Virginia 23173*  
<sup>aj</sup>*Universita' di Roma Tor Vergata, 00133 Rome Italy*  
<sup>ak</sup>*Skobeltsyn Institute of Nuclear Physics, Lomonosov Moscow State University, 119234 Moscow, Russia*  
<sup>al</sup>*University of South Carolina, Columbia, South Carolina 29208*  
<sup>am</sup>*Temple University, Philadelphia, PA 19122*  
<sup>an</sup>*Thomas Jefferson National Accelerator Facility, Newport News, Virginia 23606*  
<sup>ao</sup>*Universidad Técnica Federico Santa María, Casilla 110-V Valparaíso, Chile*  
<sup>ap</sup>*Edinburgh University, Edinburgh EH9 3JZ, United Kingdom*  
<sup>aq</sup>*University of Glasgow, Glasgow G12 8QQ, United Kingdom*  
<sup>ar</sup>*Virginia Tech, Blacksburg, Virginia 24061-0435*  
<sup>as</sup>*University of Virginia, Charlottesville, Virginia 22901*  
<sup>at</sup>*College of William and Mary, Williamsburg, Virginia 23187-8795*  
<sup>au</sup>*Yerevan Physics Institute, 375036 Yerevan, Armenia*

---

## Abstract

Photon beam asymmetry  $\Sigma$  measurements for  $\omega$  photoproduction in the reaction  $\vec{\gamma}p \rightarrow \omega p$  are reported for photon energies from 1.152 to 1.876 GeV. Data were taken using a linearly-polarized tagged photon beam, a cryogenic hydrogen target, and the CLAS spectrometer in Hall B at Jefferson Lab. The measurements obtained markedly increase the size of the database for this observable, extend coverage to higher energies, and resolve discrepancies in previously published data. Comparisons of these new results with predictions from a chiral-quark-based model and from a dynamical coupled-channels model indicate the importance of interferences between  $t$ -channel meson exchange and  $s$ - and  $u$ -channel contributions, underscoring sensitivity to the nucleon resonances included in those descriptions. Comparisons with the Bonn-Gatchina partial-wave analysis indicate the  $\Sigma$  data reported here help to fix the magnitudes of the interference terms between the leading amplitudes in that calculation (Pomeron exchange and the resonant portion of the  $J^P = 3/2^+$  partial wave), as well as the resonant portions of the smaller partial waves with  $J^P = 1/2^-, 3/2^-,$  and  $5/2^+$ .

*Keywords:* meson photoproduction; omega photoproduction; polarization observable; beam asymmetry  
*PACS:* 13.60.Le, 14.20.Dh, 14.20.Gk

---

## 1. Introduction

As a composite system of quarks and gluons, the nucleon has an excitation spectrum largely dictated by the underlying dynamics of the strong interaction. Thus, ideally, a description of the excited states of the nucleon should arise naturally from a theory built from quantum chromodynamics (QCD). However, nearly a half-century of experimental and theoretical study has not produced either a satisfactory theoretical description or a full empirical inventory of the states present in the nucleon resonance spectrum. The current understanding of the shortcomings of these efforts (as reviewed in, e.g., Refs. [1–6]) could be summarized by the provocative title of a classic paper from over thirty years ago: “Where have all the resonances gone?” [7]. The answer those authors supplied to that question remains part of the current lore today: many of the “missing resonances” are likely coupled to channels with far smaller strengths than those states that are coupled to pion-nucleon final states.

Meson photoproduction has proven to be a very productive tool for clarifying details of the nucleon resonance spectrum, complementing other approaches in the search for missing resonances. Theoretical analyses of the existing database for nucleon excited states have usually included Breit-Wigner fits to observables in order to extract masses

and widths of resonances putatively seen in the experimental results. Such analyses have shown the nucleon resonance spectrum to possess many broad and overlapping excitations, making progress difficult. Nonetheless, with respect to the mystery of the missing resonances, the current ambiguities in the nucleon resonance spectrum may still reflect the fact that the experimental database for the nucleon remains dominated by studies of  $\pi N$  final states, as implied in 1980 by Koniuk and Isgur [7].

Over the past two decades, new experimental facilities have become available, permitting experiments targeting  $\eta N$ ,  $K\Lambda$ , and  $K\Sigma$  final states. These studies have greatly expanded knowledge of nucleon resonances, as summarized in the reviews noted above [1–6]. Though many experiments have now investigated photoproduction of  $\eta N$ ,  $K\Sigma$ , and  $K\Lambda$  final states, the reaction for  $\omega$  photoproduction on the nucleon remains relatively unexplored, even though experiments focused on observables for that reaction can address several unique theoretical interests. For example, since the threshold for  $\omega$  photoproduction (1.108 GeV) lies above the thresholds for  $\pi$  and  $\eta$  photoproduction, the reaction probes the higher-mass nucleon resonances in the so-called third resonance region, where the  $\pi N$  and  $\eta N$  photoproduction cross sections have become considerably smaller than at lower energies. As in  $\eta$  photoproduction,

the isoscalar nature of the  $\omega$  means that  $\omega p$  final states can provide an “isospin filter” for the nucleon resonance spectrum, selecting only isospin  $I = \frac{1}{2}$  excitations. But, in contrast to the spinless isoscalar  $\eta$  and  $\eta'$  mesons and isovector  $\pi$  mesons, the  $\omega$  has an intrinsic spin of 1, yielding a richer set of angular momentum combinations for intermediate states. As a practical matter for experiments, the  $\omega$  has a much smaller intrinsic width ( $\Gamma=8.49$  MeV) than the  $\rho$  ( $\Gamma=149.1$  MeV), although both mesons have similar masses [8]. The narrower width for the  $\omega$  aids greatly in identifying that meson in missing-mass reconstructions. Furthermore, the principal decay mode for the  $\omega$  meson ( $\pi^+\pi^-\pi^0$  with a branching ratio of 89.2% [8]) includes two charged pions, whose relative ease in detection also facilitates reconstruction.

All these features of  $\omega$  photoproduction have stimulated theorists using a variety of approaches to harvest information from this particular channel [9–20]. Differential cross sections for meson photoproduction form the bulk of the database for baryon spectroscopy, and a number of experiments have provided data for  $\omega$  photoproduction on the proton [21–33]. However, differential cross sections alone are insufficient to deconvolute the nucleon resonance spectrum. Polarization observables in meson photoproduction, where selection of the orientations of the initial spins of the nucleon and photon, as well as measurements of the orientation of the intrinsic angular momentum of particles in the final state, give additional insight into the details of the reaction mechanism [34–36]. Such observables can arise from interferences between contributing amplitudes, consequently demanding much more specificity about the properties of the hypothesized resonance states involved in the reaction than the differential cross sections.

The photon beam asymmetry  $\Sigma$  is one such polarization observable. As discussed in Ref. [37],  $\Sigma$  for vector meson photoproduction on a nucleon is obtained with a linearly-polarized photon beam incident on an unpolarized target. Using a coordinate system where the  $z$ -axis is defined by the incoming photon direction, this observable can be expressed in the center-of-mass frame as

$$\frac{d\sigma}{d\Omega} = \frac{d\sigma_0}{d\Omega} [1 - P_\gamma \Sigma \cos\{2(\varphi - \alpha)\}], \quad (1)$$

where  $\frac{d\sigma}{d\Omega}$  is the differential cross section for the reaction using a polarized photon beam,  $\frac{d\sigma_0}{d\Omega}$  is the *unpolarized* differential cross section,  $P_\gamma$  is the degree of linear polarization of the photon beam,  $\varphi$  is the azimuthal angle of the photoproduced meson relative to a plane parallel to the floor in the laboratory frame, and  $\alpha$  is the azimuthal angle between the photon beam polarization plane and the laboratory floor plane. Predictions of  $\Sigma$  show that this observable is very sensitive to the details of which resonances are involved in the  $\gamma p \rightarrow \omega p$  reaction [9, 10, 15, 18]. However, the three published sets of measurements of  $\Sigma$  for this reaction [30, 38, 39], which have yielded a total of 74 data points, are often in conflict with each other.

The results of the experiment described in this report markedly increase the database for  $\Sigma$  by adding nearly four times more data points and extending coverage to higher incident photon energies. These new data possess finer energy and angle resolution, and resolve discrepancies among the previously published results. The measurements reported here also should motivate new theoretical analyses of this reaction that will further clarify the nucleon resonance spectrum.

## 2. Experiment

This experiment was part of a program carried out in Experimental Hall B at the Thomas Jefferson National Accelerator Facility (Jefferson Lab) in order to provide the large set of observables for exclusive meson photoproduction needed to better understand the nucleon resonance spectrum. The results reported here are based on analyses of data taken during the “g8b” running period at that facility. Data for  $\Sigma$  for  $\pi^+$ ,  $\pi^0$ ,  $\eta$ , and  $\eta'$  photoproduction from the same running period were extracted and reported previously [40–42]. Those publications provide details of the experiment and running conditions, which we summarize here.

The linearly-polarized photon beam was generated by coherent bremsstrahlung of the primary Jefferson Lab electron beam incident on a diamond radiator [43]. In coherent bremsstrahlung, the normal bremsstrahlung spectrum is enhanced at specific photon energies due to the lattice excitations within the oriented crystal. Intensity enhancements in the resulting photon spectrum above the normal bremsstrahlung spectrum possess significant polarization. The peak corresponding to the highest-energy polarized photons is called the coherent edge. By adjusting the orientation of the diamond radiator with respect to the incident electron beam, the polarization vector of the photon beam can be rotated and the energy of the coherent edge can be adjusted.

For this work, a 4.55-GeV electron beam scattering from the crystal planes of a 50- $\mu\text{m}$ -thick diamond radiator produced the linearly-polarized photons, with a remotely-controlled goniometer used to adjust the polarization direction. The degree of linear polarization for the photon beam was estimated with a calculation that used knowledge of the goniometer orientation and the geometry of the full beam line, including the degree of collimation of the photon beam, during each portion of the data collection period [44]. Timing information and energy definition for the polarized photons were obtained using the bremsstrahlung photon tagger in Hall B [45].

The photon beam impinged on a 40-cm-long liquid hydrogen target located 20 cm upstream of the center of the CEBAF Large Acceptance Spectrometer (CLAS) [46]. CLAS consists of six (ideally) identical charged-particle magnetic spectrometers contained within a superconducting toroidal magnet that generates an approximately azimuthal magnetic field distribution. Information from the

CLAS subsystems was analyzed to provide four-momentum and reaction vertex information event-by-event for each charged particle originating in the cryogenic target region and passing through the tracking regions of the spectrometer. For these measurements, data from the drift-chamber subsystem for tracking charged particles [47], the time-of-flight subsystem [48], and a plastic scintillator array surrounding the cryogenic target (which determined when charged particles passed from the target into the drift chamber region) [49], provided the primary information for determining the four-momenta of the recoil proton, the photoproduced mesons, and their decay products.

The running period was split into intervals of approximately one week during which data were taken at a specific setting of the coherent-edge energy. The coherent-edge settings were 1.3, 1.5, 1.7, and 1.9 GeV. Approximately every hour within each interval, the polarization plane for the  $\vec{E}$ -field of the photon beam was adjusted to either be parallel to the floor or perpendicular to the floor in order to minimize the effects of any change in the CLAS acceptance within a coherent-edge setting. Measurements where the same photon energy was present in adjacent coherent-edge settings were used to check for consistency in polarization estimates for a given photon energy. These consistency checks indicated that the uncertainty in the photon beam polarization was 6%, as noted in Ref. [40]. Runs with an amorphous carbon radiator were also taken periodically during each interval to provide data for unpolarized photons. The use of the amorphous radiator and alternate polarization orientations reduced systematic uncertainties arising from the non-uniform CLAS acceptance for the charged decay products of the  $\omega$  meson through the comparison of combinations of the data from the different polarization orientations with data from the amorphous radiator.

### 3. Data reduction and analysis

For each charged-particle track seen in CLAS, the measured speed  $v$ ,  $\beta = v/c$ , and three-momentum were used for particle identification via the GPID algorithm [40, 41, 50]. That algorithm compares the measured  $\beta$  of the particle whose identity is to be determined with estimated values of  $\beta$  based on hypothetical identities for that particle. The hypothetical particle identity that provided a  $\beta$  value closest to the measured  $\beta$  was then assigned to that particle. A visualization of the performance of this technique may be seen in Fig. 1 of Ref. [40].

With the identity of each scattered particle established, corrections were made for the energy lost by each scattered charged particle as that particle passed through the materials in the cryogenic target and the CLAS detector with the CLAS ELOSS program [51]. The timing information for each charged-particle track was used to determine the time when that track originated in the target (i.e., the vertex time). Independently, the timing information of each electron detected at the focal plane of the tagger was

used to determine the time when the corresponding bremsstrahlung photon arrived at the vertex (photon time). The photon whose photon time most closely matched with the vertex time was selected as the photon that caused the reaction. This selection was important because the intensity of the electron beam impacting the radiator of the photon tagger was such that multiple photons could arise from a single pulse of beam electrons. Events were rejected where an additional photon was within  $\pm 1$  ns of the selected photon in order to avoid any ambiguity in determining which photon caused the reaction.

The kinematic quantities determined from the time-of-flight and drift-chamber systems yielded good definition of the four-momenta for the  $p$ ,  $\pi^+$ , and  $\pi^-$  particles scattered into CLAS. Nonetheless, to simultaneously correct for imperfections in the map for the magnetic field of CLAS, momentum corrections for tracks were determined by demanding four-momentum conservation in a kinematic fit of a large sample of  $\gamma p \rightarrow \pi^+ \pi^- p$  events seen in the spectrometer where all three final-state particles were detected, in the same manner as discussed in Ref. [42].

Based on the assumption that the reaction observed was  $\gamma p \rightarrow pX$ , the polar scattering angle and the magnitude of the three-momentum for the proton recoiling from meson photoproduction can be used to calculate the mass  $M_X$  of the missing state  $X$ . As seen in the upper panel of Fig. 1, however, a sizeable background in the missing-mass spectrum for  $\gamma p \rightarrow pX$  appears under the peak associated with photoproduction of the  $\omega$  meson due to multi-pion and  $\rho$  meson photoproduction. This background was reduced by requiring that the recoil proton and charged pions resulting from the decay  $\omega \rightarrow \pi^+ \pi^- \pi^0$  were detected in CLAS, and then identifying a neutral meson by assuming the decay  $\omega \rightarrow \pi^+ \pi^- Y$  with the restriction on the missing mass  $M_Y = M(\pi^0)$ . This requirement effectively removed contributions from  $\rho$  photoproduction and significantly reduced the background beneath the photoproduced  $\omega$  peak, as exemplified in the lower panel of Fig. 1. The remaining background is attributable primarily to multi-pion photoproduction, which was removed to extract the  $\omega$  yield as described below.

These  $\omega$  missing-mass spectra were then split into 27-MeV-wide bins in photon energy. Incorporating the results of the kinematic fit described above, the centroids for each of the photon energy bins used in this analysis were determined to an accuracy that was typically better than  $\pm 0.1$  MeV, and always better than  $\pm 0.5$  MeV. These binned spectra were then analyzed as in Refs. [40, 41] with a Fourier-moment method to extract the beam asymmetry as a function of the center-of-mass meson scattering angle  $\cos(\theta_{c.m.}^\omega)$  for the specific incident photon energy  $E_\gamma$  bins (and, consequently, center-of-mass  $W$  bins) chosen for this analysis. Cosine- $n\varphi$ -moment histograms (where  $n=0, 2, 4$ ) were constructed by taking each  $\omega$  event in the missing-mass histograms and weighting that event by the value of  $\cos n\varphi$  corresponding to that event. With this approach, events within a particular  $\cos(\theta_{c.m.}^\omega)$  bin for  $\varphi$  are

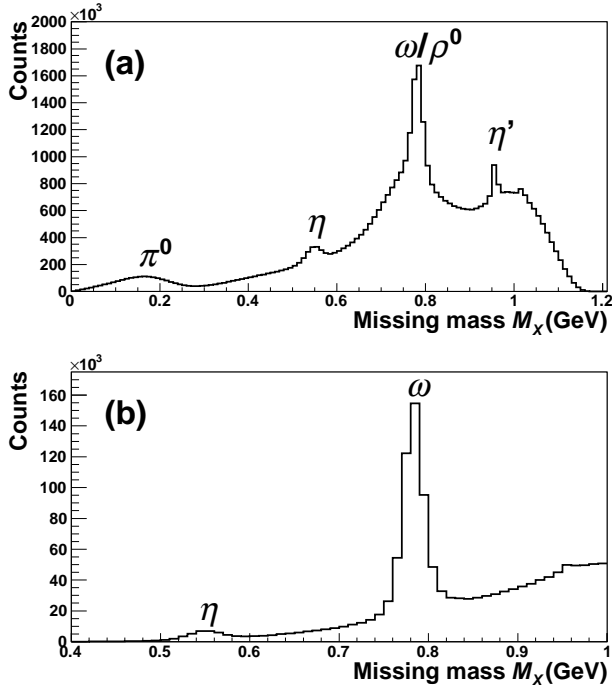


Figure 1: Missing mass  $M_X$  for the reaction  $\gamma p \rightarrow pX$  for the 1.9-GeV coherent-edge setting, with peaks corresponding to various photoproduced mesons. Upper panel: Full missing-mass spectrum. Lower panel: Missing-mass spectrum for the reaction  $\gamma p \rightarrow pX$  requiring  $X \rightarrow \pi^- \pi^+ \pi^0$ , as described in the text.

combined simultaneously to determine  $\Sigma$ . Applying this Fourier-moment method to  $\Sigma$ , the resulting equation for the beam asymmetry may be written as

$$\Sigma = \frac{\tilde{Y}_{\perp 2} - \tilde{Y}_{\parallel 2}}{\frac{P_{\parallel}}{2}(\tilde{Y}_{\perp 0} + \tilde{Y}_{\perp 4}) + \frac{P_{\perp}}{2}(\tilde{Y}_{\parallel 0} + \tilde{Y}_{\parallel 4})}, \quad (2)$$

where  $\tilde{Y}_{\perp n}(\tilde{Y}_{\parallel n})$  is the background-subtracted meson yield for a photon beam with polarization vector perpendicular (parallel) to the laboratory floor, normalized by the number of incident photons for that particular polarization orientation, with each event weighted according to the Fourier moment  $\cos n\varphi$ , and  $P_{\perp}(P_{\parallel})$  is the degree of photon polarization. The numerator and denominator in Eq. 2 were constructed for each kinematic bin. For each Fourier-moment histogram within a kinematic bin, the meson yield was determined by removing the background under the  $\omega$  meson peak. Since the  $\omega$  peak shows up very clearly in such histograms, this background subtraction was accomplished by fitting each of the Fourier-moment histograms with the combination of a second-order polynomial shape (describing the multi-pion background) and a Gaussian (describing the  $\omega$  peak). The background was well-described by the polynomial shape, and the uncertainty in the background was given by the uncertainty in this shape determined by the fit. The  $\omega$  yield for that particular histogram was then obtained by subtracting the polynomial from the original distribution and then summing the remaining events within the area of the  $\omega$  peak.

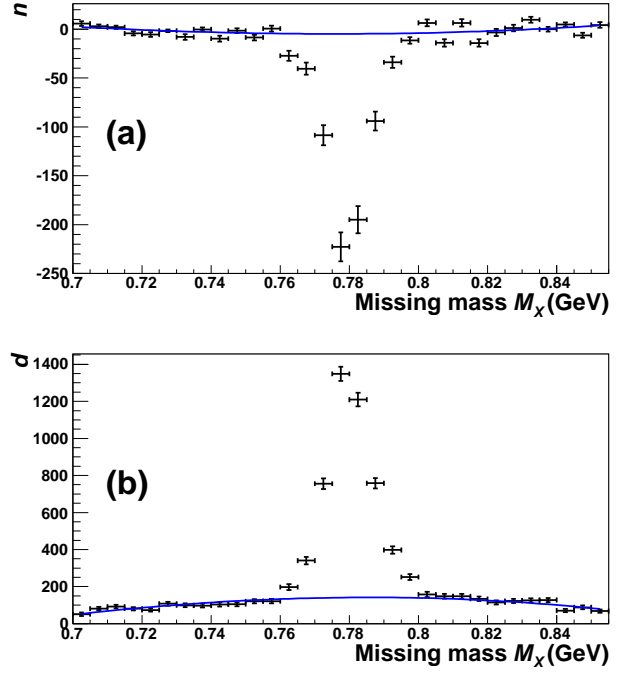


Figure 2: Example of yield extraction for the numerator  $n$  (upper panel) and denominator  $d$  (lower panel) defined by Eq. 2 for  $E_{\gamma}=1.314$  GeV and  $\cos(\theta_{c.m.}^{\omega}) = -0.55$ . The solid line indicates the background fit discussed in the text.

Examples of Fourier-moment histograms with background fits are shown in Fig. 2. Finite-size bin corrections for extracted  $\Sigma$  values are also addressed with this method, as described in Ref. [40]. Using preliminary estimates of the spin-density matrix elements for  $\omega$  decay [52], the values of  $\Sigma$  also were corrected to account for CLAS acceptance variations for charged pions due to any polarization transferred to those pions in the  $\omega$  decay.

#### 4. Statistical and systematic uncertainties

A statistical uncertainty for  $\Sigma$  was determined for each kinematic bin, based on the definition in Eq. 2. With that definition, many experimental quantities (e.g., acceptance, target thickness, single-particle detection efficiencies) canceled in Eq. 2 so that the uncertainty for a particular kinematic bin was to a great extent dictated by statistical uncertainties in the  $\omega$  yield for that bin [40, 41]. The relative normalization of the photon flux for the different coherent-edge settings and polarization orientations had statistical uncertainties much less than 1%, contributing negligibly to the overall uncertainty in  $\Sigma$ . The effects arising from polarization transfer to the charged pions from  $\omega$  decay used to reconstruct the  $\omega$  provided an additional statistical uncertainty in  $\Sigma$  for each kinematic bin, which was conservatively set to 0.01 for all kinematic bins based on those simulations. This uncertainty due to polarization transfer was then added in quadrature to the statistical

uncertainty in  $\Sigma$  from Eq. 2 to arrive at the overall statistical uncertainty for that kinematic bin.

The systematic uncertainties for all values of  $\Sigma$  obtained at a particular photon energy  $E_\gamma$  arose from the uncertainties in the polarization of the photon beam and the relative flux normalization for that particular photon energy. By analyzing  $\Sigma$  measurements for the same  $E_\gamma$  taken at different coherent-edge settings, as noted above, the systematic uncertainty in the photon beam polarization for a particular polarization orientation was found to be 4%, as reported in Ref. [40]. Since two different polarization orientations are combined to obtain  $\Sigma$ , and the photon-beam flux contributions are negligible, adding the two polarization uncertainties in quadrature resulted in an estimated systematic uncertainty in  $\Sigma$  of 6% for all photon energies, as given in Refs. [40, 41].

## 5. Results and comparisons with prior results

The results for  $\Sigma$  obtained here [53] are shown in Fig. 3. The uncertainty shown at each point is the statistical uncertainty in  $\Sigma$  described in Sect. 4. Additionally, the entire  $\Sigma$  distribution at each center-of-mass energy  $W$  shown in Fig. 3 possesses the 6% systematic uncertainty due to the uncertainty in the polarization of the photon beam noted in Sect. 4.

The published results for  $\Sigma$  from the CBELSA/TAPS collaboration [38] and the GRAAL collaboration [30, 39] are also shown in Fig. 3. The data reported here extend knowledge of this observable well beyond the  $W$  range studied in those previous experiments, and generally have higher precision. The energy-bin width here (typically  $\sim 27$  MeV) is considerably smaller than that for the previous studies (typically  $\sim 100$  MeV). Near threshold where observables change rapidly, the better energy resolution of the current study will prove very useful to future analyses of the nucleon resonance spectrum. Angular resolution is also much better in the current results, which will enable more detailed comparisons with the theoretical predictions below.

As is clear from Fig. 3, our results and the previous measurements of  $\Sigma$  indicate that this observable is negative and significantly different from zero near  $\cos(\theta_{c.m.}^\omega)=0$ . This general observation will be of interest to the discussion in the next section. With respect to the shape of  $\Sigma$  as a function of  $\cos(\theta_{c.m.}^\omega)$ , all measurements suggest a generally similar angular dependence for  $\Sigma$ . In more detail, the overall agreement with the CBELSA/TAPS results [38] is good for all energies reported in that work, though the experimental uncertainties are much larger for that earlier work than the uncertainties in the results reported here. On the other hand, the results reported here generally do not agree with those from the GRAAL publications except at the most forward and most backward angles where  $\Sigma$  approaches zero. The older results from GRAAL [30] generally are smaller in magnitude than the data reported here. The data reported here also disagree

with the newer GRAAL measurements [39] at intermediate angles by a factor of about 2. Furthermore, at about  $E_\gamma \geq 1.3$  GeV, the two GRAAL publications appear to disagree with each other at intermediate angles. The results from both GRAAL publications generally disagree with the results from CBELSA/TAPS at most intermediate angles. Since the angular dependence of  $\Sigma$  in both GRAAL datasets appears similar to that measured here and by CBELSA/TAPS, and since the CBELSA/TAPS results agree with the results reported here, the observed discrepancies between our results and GRAAL may be due to an unknown systematic effect in the yield extraction for the more recent GRAAL publication. Regardless, our data weigh in favor of the CBELSA/TAPS results versus the GRAAL measurements.

## 6. Comparison with theoretical predictions

When coupled with measurements of other observables and/or other reactions, these new data can provide important tests and constraints for theoretical predictions of the nucleon resonance spectrum. As examples for this discussion, three different approaches are compared with these new  $\Sigma$  data. In these comparisons, the reader should note that large  $\Sigma$  values at intermediate angles are not produced by  $t$ -channel exchange, but rather must arise from contributions from the  $s$ - and  $u$ - channels [9, 10, 18]. This makes measurements at those angles especially useful in testing contributions of nucleon resonances.

The first set of predictions provided here (denoted CQM hereafter) used a  $SU(6) \otimes SU(3)$  constituent-quark model with an effective chiral Lagrangian approach for the reaction dynamics [9–12, 54, 55]. The Lagrangian for the quark- $\omega$  coupling utilized a non-relativistic constituent-quark treatment for the nucleon. Thus, as suggested in Sect. 1, such an approach is an approximation to the idealized fundamental quark-level description of the nucleon in terms of QCD. The CQM consisted of three pieces:  $s$ - and  $u$ -channel nucleon exchange,  $t$ -channel Pomeron (natural parity) exchange, and  $t$ -channel  $\pi^0$  (unnatural parity) exchange. In this model, with respect to the comment above concerning large values of  $\Sigma$  at intermediate angles, those large asymmetries cannot be produced by Pomeron and/or  $\pi^0$  exchanges, but rather must arise through the interference between (1) the Pomeron and/or  $\pi^0$  exchange and (2) the ( $s$ - and  $u$ -channel) effective Lagrangian nucleon exchange. The tree-level diagrams were calculated explicitly in this approach, and the quark-model wavefunctions for the nucleons and baryon resonances provided a form factor for the interaction vertices. Consequently, all of the  $s$ - and  $u$ -channel resonances could be consistently included to facilitate searching for “missing resonances.” A set of eight well-known resonances expressed in terms of their representations in  $SU(6) \otimes SU(3)$  were included. Specifically, those resonances were the  $N(1440)1/2^+$ ,  $N(1520)3/2^-$ ,  $N(1535)1/2^-$ ,  $N(1680)5/2^+$ ,  $N(1710)1/2^+$ ,  $N(1720)3/2^+$ ,  $N(1900)3/2^+$ , and  $N(2000)5/2^+$ .

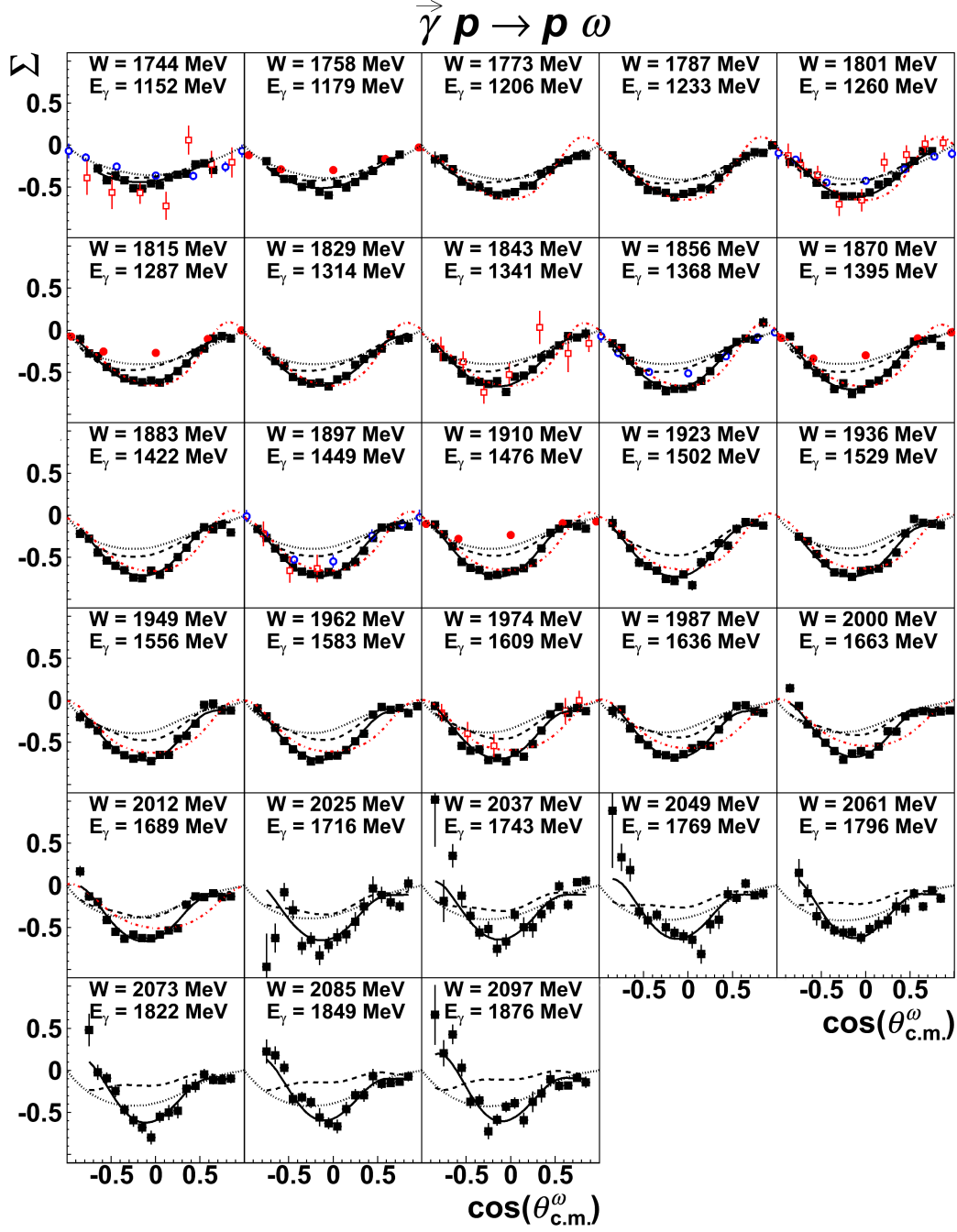


Figure 3: (Color online) Photon beam asymmetry  $\Sigma$  as a function of  $\cos(\theta_{c.m.}^{\omega})$  for  $\vec{\gamma}p \rightarrow \omega p$  for  $E_{\gamma}$  from 1.152 GeV ( $W=1.744$  GeV) to 1.876 GeV ( $W=2.097$  GeV). Uncertainties for data reported here (black squares) are statistical for each point shown, and do not include a 6% systematic uncertainty at each energy. Also shown are results from CBELSA/TAPS (open red squares [38]) and GRAAL (blue open circles [30] and red solid circles [39]). The predictions described in the text by CQM (black dotted lines) and CCA (red dotted-dashed lines), as well as new fits with the Bonn-Gatchina formalism discussed in the text (black dashed and black solid lines), are also shown.

The CQM predictions [54] are compared with the results from this and prior experiments in Fig. 3. As noted above, any large observed asymmetry in the CQM results must arise through interference effects between Pomeron and/or  $\pi^0$   $t$ -channel exchange and the  $s$ - and  $u$ -channel contributions. Hence, the general observation above that all measurements of  $\Sigma$  in Fig. 3 are significantly different from zero at intermediate angles implies that such interferences indeed are present and are critical to understanding the data for all energies studied here. Next, we note that the parameters in CQM were adjusted [54] to fit the older GRAAL data [30]. The CQM predictions therefore do not consider more recent data. Thus, as expected from the discussion of previously published data, where the older GRAAL data exist, the CQM predictions markedly underpredict the data reported here. However, simply multiplying the predictions by a factor of 2 at those energies results in a prediction very close in magnitude and shape to the data reported here. This suggests that the resonances used and the interferences found in Refs. [9–12] could still be mostly correct, aside from the constants used to fix the magnitudes of the various terms to fit the older GRAAL data. The CQM calculation indicated that the  $N(1720)3/2^+$  played the major role in the shape of the angular dependence seen for  $\Sigma$  near threshold to about  $W=1.9$  GeV. Given the interest in quark-based descriptions of the nucleon and the suggestive agreement seen between the shape of the angular dependence in the CQM predictions and this new data, an updated fit with this approach would be interesting.

A second set of predictions for  $\Sigma$  used a coupled-channels approach (denoted CCA hereafter) where pion- and photon-induced reactions were considered simultaneously while unitarity was preserved [18]. We were provided predictions for  $E_\gamma=1.206$  to 2.012 GeV [56]. The CCA formalism was one component of a program of analyses for electromagnetic meson production data at Jefferson Lab’s Excited Baryon Analysis Center. The CCA predictions for  $\pi$  and  $\omega$  production employed a set of six intermediate channels ( $\pi N$ ,  $\eta N$ ,  $\pi\Delta$ ,  $\sigma N$ ,  $\rho N$ ,  $\omega N$ ), and incorporated off-shell effects using the dynamical coupled-channel method developed by Matsuyama, Sato, and Lee [57]. A large value for  $\Sigma$  in this model required  $s$ - and  $u$ -channel contributions in one or more partial-waves for the  $\omega N$  intermediate state. The incorporation of the  $\omega N$  intermediate state was found to produce marked changes in the  $D_{15}$  partial-wave amplitude, underscoring the importance of considering multiple channels and reactions simultaneously. The predictions for the unpolarized differential cross sections for  $\gamma p \rightarrow \omega p$  that were incorporated in the fit were in very good agreement with published data [28].

Though a large database of about 1800 data points was incorporated in the CCA fit, no  $\Sigma$  data for  $\bar{\gamma}p \rightarrow \omega p$  were included in the fit. The CCA results thus represented a true prediction for that observable. When the CCA predictions of Ref. [18] were compared to the only  $\Sigma$  data existing at that time (the older GRAAL data [30]), the calculation

predicted  $\Sigma$  with a magnitude greater than those data except at the lowest energy. By contrast, as seen in Fig. 3, the same CCA predictions agree well with the new data reported here [18, 56]. Given that CCA simultaneously fits six different channels with good success, the agreement seen in Fig. 3 suggests the model likely is correct in much of its description of the underlying dynamics for the various reaction channels. While the CQM model indicated that the  $N(1720)3/2^+$  resonance was critical to understanding  $\Sigma$  near threshold, CCA found instead that the  $D_{13}$  partial-wave amplitude, using resonances with bare masses of 1.899 GeV and 1.988 GeV, were the most significant component in generating the asymmetry. Given the importance of multi-channel coupling effects, the disagreement between CQM and CCA perhaps lies in a failure of the CQM calculations to respect unitarity in the  $\gamma p$  reactions. Updating the CCA work with this new data could clarify resonance contributions for  $W < 2$  GeV.

A third set of calculations was developed for this publication by the Bonn-Gatchina group (denoted here as BG) from their partial-wave analysis [17, 20, 58]. The BG analysis incorporates a large database (more than 2000 data points) of differential cross sections and spin observables from pion- and photon-induced reactions on the nucleon. This approach makes use of dispersion relations based on the  $N/D$  technique, corresponding to the solution of the Bethe–Salpeter equation with separable interactions. Consistent in part with the CQM results noted above, a recent analysis with the BG approach of  $\omega$  photoproduction using newly-available data on the  $E$  and  $G$  spin observables found that the  $J^P=3/2^+$  partial wave provided the strongest contributions to describing correctly the  $W$  behavior of spin observables [59]. The Pomeron exchange contribution amounted to nearly half the total cross section for the  $\gamma p \rightarrow \omega p$  at  $W=2$  GeV.

Fig. 3 shows the results from these new fits using the BG approach with (black solid line) and without (black dashed line) considering the data reported here, indicating the impact of these new data on the BG parameters. As illustrated by the differences seen in that figure between the original BG predictions and those considering the data reported here, our new  $\Sigma$  data significantly change the BG predictions at all energies, with the differences becoming more pronounced as  $W$  increases. When incorporated into the new fits, the  $\Sigma$  data reported here helped refine details of the interference between the leading amplitudes in the calculation – the Pomeron exchange and the resonant portion of the  $J^P = 3/2^+$  partial wave – as well as the resonant portions of the smaller partial waves (e.g., the  $J^P = 1/2^-$ ,  $3/2^-$ , and  $5/2^+$ ). Further details and discussion of this new BG analysis will form the subject of a subsequent publication.

## 7. Conclusions

The results of the experiment reported here have provided hundreds of new high-precision data for  $\Sigma$  for the



reaction  $\bar{\gamma}p \rightarrow \omega p$ , nearly quadrupling the size of the database for this observable. The results resolve the disagreements between the previously published datasets from CBELSA/TAPS and GRAAL, where agreement between the CBELSA/TAPS results and the results reported here would suggest that the GRAAL measurements are systematically too small. Our results also extend the database for  $\Sigma$  to higher energies, facilitating explorations of nucleon excitations within that energy regime. An initial study with the BG partial-wave approach indicates these new data significantly impact the predictions for  $\Sigma$  using that approach, showing that these new data will help further refine understanding of the interference of many of the partial-wave amplitudes that contribute to the  $\omega p$  photoproduction reaction. Similar comparisons with other theoretical models will further enhance our knowledge of the nucleon resonance spectrum.

## 8. Acknowledgements

The authors express appreciation to Q. Zhao and M. Paris for providing predictions for  $\Sigma$  shown in Fig. 3. The authors gratefully acknowledge the work of the Jefferson Lab staff and financial support by the U.S. National Science Foundation, the Deutsche Forschungsgemeinschaft, the Russian Science Foundation, the Chilean Comisión Nacional de Investigación Científica y Tecnológica (CONICYT), the Italian Istituto Nazionale di Fisica Nucleare, the French Centre National de la Recherche Scientifique, the French Commissariat à l’Energie Atomique, the Scottish Universities Physics Alliance (SUPA), the United Kingdom’s Science and Technology Facilities Council, and the National Research Foundation of Korea. This material is based upon work supported by the U.S. Department of Energy, Office of Science, Office of Nuclear Physics under contract DE-AC05-06OR23177. The Southeastern Universities Research Association (SURA) operates the Thomas Jefferson National Accelerator Facility for the United States Department of Energy under contract DE-AC05-84ER40150.

## 9. References

- [1] L. Tiator, D. Drechsel, S. S. Kamalov, M. Vanderhaeghen, Electromagnetic excitation of nucleon resonances, *Eur. Phys. J. ST* 198 (2011) 141–170. doi:10.1140/epjst/e2011-01488-9.
- [2] I. G. Aznauryan, et al., Studies of nucleon resonance structure in exclusive meson electroproduction, *Int. J. Mod. Phys. E22* (2013) 1330015. doi:10.1142/S0218301313300154.
- [3] I. C. Cloet, C. D. Roberts, Explanation and prediction of observables using continuum strong QCD, *Prog. Part. Nucl. Phys.* 77 (2014) 1–69. doi:10.1016/j.pnpnp.2014.02.001.
- [4] V. Credé, W. Roberts, Progress towards understanding baryon resonances, *Rept. Prog. Phys.* 76 (2013) 076301. doi:10.1088/0034-4885/76/7/076301.
- [5] A. Bazavov, et al., Additional strange hadrons from QCD thermodynamics and strangeness freezeout in heavy-ion collisions, *Phys. Rev. Lett.* 113 (7) (2014) 072001. doi:10.1103/PhysRevLett.113.072001.
- [6] V. D. Burkert, Spectrum and structure of excited baryons with CLAS, in: *CRC-16 Symposium*, Bonn, Germany, June 6-9, 2016, 2016. arXiv:1610.00400.
- [7] R. Koniuk, N. Isgur, Where have all the resonances gone? An analysis of baryon couplings in a quark model with chromodynamics, *Phys. Rev. Lett.* 44 (1980) 845. doi:10.1103/PhysRevLett.44.845.
- [8] Particle Data Group, C. Patrignani, et al., Review of particle physics, *Chin. Phys. C40* (10) (2016) 100001. doi:10.1088/1674-1137/40/10/100001.
- [9] Q. Zhao, J. P. Didelez, M. Guidal, B. Saghai, Nucleonic resonance effects in the  $\phi$  meson photoproduction, *Nucl. Phys. A660* (1999) 323–347. doi:10.1016/S0375-9474(99)00398-X.
- [10] Q. Zhao, Nucleonic resonance excitations with linearly polarized photon in  $\gamma p \rightarrow \omega p$ , *Phys. Rev. C63* (2001) 025203. doi:10.1103/PhysRevC.63.025203.
- [11] Q. Zhao, Vector meson photoproduction in the quark model, in: *2nd International Workshop on the Physics of Excited Nucleons (NSTAR 2001)* Mainz, Germany, March 7-10, 2001, 2001. arXiv:nucl-th/0106030. URL <http://alice.cern.ch/format/showfull?sysnb=2259836>
- [12] Q. Zhao, Study  $\omega$  and  $\phi$  photoproduction in the nucleon isotopic channels, in: *Electromagnetic interactions in nuclear and hadron physics. Proceedings, International Symposium, EMI 2001, Osaka, Japan, December 4-7, 2001, 2002*, pp. 632–641. arXiv:nucl-th/0202023. URL <http://alice.cern.ch/format/showfull?sysnb=2294598>
- [13] Y.-s. Oh, T. S. H. Lee,  $\pi$  and  $\rho$  loop corrections to  $\omega$  photoproduction in the resonance region, *Nucl. Phys. A721* (2003) 743–746. doi:10.1016/S0375-9474(03)01171-0.
- [14] Y.-s. Oh, T. S. H. Lee, One-loop corrections to  $\omega$  photoproduction near threshold, *Phys. Rev. C66* (2002) 045201. doi:10.1103/PhysRevC.66.045201.
- [15] V. Shklyar, H. Lenske, U. Mosel, G. Penner, Coupled-channel analysis of the  $\omega$ -meson production in  $\pi N$  and  $\gamma N$  reactions for c.m. energies up to 2 GeV, *Phys. Rev. C71* (2005) 055206, [Erratum: *Phys. Rev. C72*, 019903(2005)]. doi:10.1103/PhysRevC.72.019903, 10.1103/PhysRevC.71.055206.
- [16] A. Usov, O. Scholten, Channel coupling effects in  $\rho$ -meson photoproduction, *Phys. Rev. C74* (2006) 015205. doi:10.1103/PhysRevC.74.015205.
- [17] A. V. Anisovich, A. V. Sarantsev, Partial decay widths of baryons in the spin-momentum operator expansion method, *Eur. Phys. J. A30* (2006) 427–441. doi:10.1140/epja/i2006-10102-1.
- [18] M. W. Paris, Dynamical coupled channel calculation of pion and omega meson production, *Phys. Rev. C79* (2009) 025208. doi:10.1103/PhysRevC.79.025208.
- [19] A. V. Sarantsev, A. V. Anisovich, V. A. Nikonov, H. Schmieden, Polarization degrees of freedom in near-threshold photoproduction of  $\omega$  mesons in the  $\pi^0\gamma$  decay channel, *Eur. Phys. J. A39* (2009) 61–70. doi:10.1140/epja/i2008-10696-0.
- [20] A. V. Anisovich, R. Beck, E. Klempt, V. A. Nikonov, A. V. Sarantsev, U. Thoma, Properties of baryon resonances from a multichannel partial wave analysis, *Eur. Phys. J. A48* (2012) 15. doi:10.1140/epja/i2012-12015-8.
- [21] Brown-Harvard-MIT-Padova-Weizmann Institute Bubble Chamber Group, Photoproduction of  $\omega^0$  Mesons, *Phys. Rev.* 155 (1967) 1468–1476. doi:10.1103/PhysRev.155.1468.
- [22] Aachen-Berlin-Bonn-Hamburg-Heidelberg-Munich Collaboration, Photoproduction of meson and baryon resonances at energies up to 5.8 GeV, *Phys. Rev.* 175 (1968) 1669–1696. doi:10.1103/PhysRev.175.1669.
- [23] Y. Eisenberg, B. Haber, Z. Carmel, E. Peleg, E. E. Ronat, A. Shapira, G. Vishinsky, R. Yaari, G. Yekutieli, Photoproduction of vector mesons and other resonances at 4.3-GeV, *Phys. Rev. Lett.* 22 (1969) 669. doi:10.1103/PhysRevLett.22.669.
- [24] J. Ballam, et al., Vector meson production by polarized photons at 2.8 GeV, 4.7-GeV, and 9.3-GeV, *Phys. Rev. D7* (1973) 3150. doi:10.1103/PhysRevD.7.3150.
- [25] R. W. Clift, J. B. Dainton, E. Gabathuler, L. S. Littenberg, R. Marshall, S. E. Rock, J. C. Thompson, D. L. Ward, G. R.

- Brookes, Observation of a baryon exchange dip and parton effects in backward photoproduction of  $\omega$ , *Phys. Lett.* B72 (1977) 144–148. doi:10.1016/0370-2693(77)90082-X.
- [26] B. Friman, M. Soyeur, Photoproduction of vector mesons off nucleons near threshold, *Nucl. Phys.* A600 (1996) 477–490. doi:10.1016/0375-9474(96)00011-5.
- [27] F. J. Klein, Overview of vector meson photoproduction, *PiN Newslett.* 14 (1998) 141–149.
- [28] J. Barth, et al., Low-energy of photoproduction of  $\omega$ -mesons, *Eur. Phys. J.* A18 (2003) 117–127. doi:10.1140/epja/i2003-10061-y.
- [29] CLAS Collaboration, M. Battaglieri, et al., Photoproduction of the  $\omega$  meson on the proton at large momentum transfer, *Phys. Rev. Lett.* 90 (2003) 022002. doi:10.1103/PhysRevLett.90.022002.
- [30] GRAAL Collaboration, J. Ajaka, et al., Evidence for nucleon-resonance excitation in  $\omega$ -meson photoproduction, *Phys. Rev. Lett.* 96 (2006) 132003. doi:10.1103/PhysRevLett.96.132003.
- [31] CLAS Collaboration, M. Williams, et al., Differential cross sections and spin density matrix elements for the reaction  $\gamma p \rightarrow p\omega$ , *Phys. Rev.* C80 (2009) 065208. doi:10.1103/PhysRevC.80.065208.
- [32] LEPS Collaboration, M. Sumihama, et al., Backward-angle  $\eta$  photoproduction from protons at  $E(\gamma) = 1.6 - 2.4$  GeV, *Phys. Rev.* C80 (2009) 052201. doi:10.1103/PhysRevC.80.052201.
- [33] CB-ELSA and TAPS Collaboration, A. Wilson, et al., Photoproduction of  $\omega$  mesons off the proton, *Phys. Lett.* B749 (2015) 407–413. doi:10.1016/j.physletb.2015.08.011.
- [34] I. S. Barker, A. Donnachie, J. K. Storrow, Complete experiments in pseudoscalar photoproduction, *Nucl. Phys.* B95 (1975) 347–356. doi:10.1016/0550-3213(75)90049-8.
- [35] W. M. Kloet, W.-T. Chiang, F. Tabakin, Spin information from vector-meson decay in photoproduction, *Phys. Rev.* C58 (1998) 1086–1097. doi:10.1103/PhysRevC.58.1086.
- [36] W. Roberts, T. Oed, Polarization observables for two-pion production off the nucleon, *Phys. Rev.* C71 (2005) 055201. doi:10.1103/PhysRevC.71.055201.
- [37] M. Pichowsky, C. Savkli, F. Tabakin, Polarization observables in vector meson photoproduction, *Phys. Rev.* C53 (1996) 593–610. doi:10.1103/PhysRevC.53.593.
- [38] CB-ELSA and TAPS Collaboration, F. Klein, et al., Beam asymmetries in near threshold  $\omega$  photoproduction off the proton, *Phys. Rev.* D78 (2008) 117101. doi:10.1103/PhysRevD.78.117101.
- [39] GRAAL Collaboration, V. Vegna, et al., Measurement of the  $\Sigma$  beam asymmetry for the  $\omega$  photo-production off the proton and the neutron at GRAAL, *Phys. Rev.* C91 (6) (2015) 065207. doi:10.1103/PhysRevC.91.065207.
- [40] CLAS Collaboration, M. Dugger, et al., Beam asymmetry  $\Sigma$  for  $\pi^+$  and  $\pi^0$  photoproduction on the proton for photon energies from 1.102 to 1.862 GeV, *Phys. Rev.* C88 (6) (2013) 065203, [Addendum: *Phys. Rev.* C89, no. 2, 029901 (2014)]. doi:10.1103/PhysRevC.88.065203, 10.1103/PhysRevC.89.029901.
- [41] CLAS Collaboration, P. Collins, et al., Photon beam asymmetry  $\Sigma$  for  $\eta$  and  $\eta'$  photoproduction from the proton, *Phys. Lett.* B771 (2017) 213–221. doi:10.1016/j.physletb.2017.05.045.
- [42] M. Dugger, C. Hanretty, Correction to the incident photon energy for g8b data, CLAS-Note 2009-030, CLAS Collaboration, Jefferson Lab (2010). URL <https://misportal.jlab.org/ul/physics/hall-b/clas/viewFile.cfm/2009-030.pdf?documentId=605>
- [43] H. Bilokon, G. Bologna, F. Celani, B. D’Ettorre-Piazzoli, R. Falcioni, G. Mannocchi, P. Picchi, Coherent bremsstrahlung in crystals as a tool for producing high-energy photon beams to be used in photoproduction experiments at CERN SPS, *Nucl. Instrum. Meth.* 204 (1983) 299. doi:10.1016/0167-5087(83)90061-3.
- [44] K. Livingston, Polarization for coherent bremsstrahlung enhancement, CLAS-Note 2011-020, CLAS Collaboration, Jefferson Lab (2011). URL <http://www.nuclear.gla.ac.uk/~kl/mainz/cbrem/FittingCoherentBrem.pdf>
- [45] D. I. Sober, et al., The bremsstrahlung tagged photon beam in Hall B at JLab, *Nucl. Instrum. Meth.* A440 (2000) 263–284. doi:10.1016/S0168-9002(99)00784-6.
- [46] B. A. Mecking, et al., The CEBAF Large Acceptance Spectrometer (CLAS), *Nucl. Instrum. Meth.* A503 (2003) 513–553. doi:10.1016/S0168-9002(03)01001-5.
- [47] M. D. Mestayer, et al., The CLAS drift chamber system, *Nucl. Instrum. Meth.* A449 (2000) 81–111. doi:10.1016/S0168-9002(00)00151-0.
- [48] E. S. Smith, et al., The time-of-flight system for CLAS, *Nucl. Instrum. Meth.* A432 (1999) 265–298. doi:10.1016/S0168-9002(99)00484-2.
- [49] Y. G. Sharabian, et al., A new highly segmented start counter for the CLAS detector, *Nucl. Instrum. Meth.* A556 (2006) 246–258. doi:10.1016/j.nima.2005.10.031.
- [50] E. Pasyuk, Brief user guide for GPID, CLAS-Note 2007-008, CLAS Collaboration, Jefferson Lab (2007). URL <http://www1.jlab.org/ul/Physics/Hall-B/clas/public/2007-008.pdf>
- [51] E. Pasyuk, Energy loss corrections for charged particles in CLAS, CLAS-Note 2007-016, CLAS Collaboration, Jefferson Lab (2007). URL <https://misportal.jlab.org/ul/physics/hall-b/clas/viewFile.cfm/2007-016.pdf?documentId=423>
- [52] B. Vernarsky, First measurements of the  $\rho^3$  spin density matrix elements in  $\gamma p \rightarrow p\omega$  using CLAS at JLAB, *Int. J. Mod. Phys. Conf. Ser.* 26 (2014) 1460063. doi:10.1142/S2010194514600635.
- [53] Data reported here may be accessed in the CLAS Physics Database at <http://clas.sinp.msu.ru/cgi-bin/jlab/db.cgi>.
- [54] Q. Zhao, Private communication (2016).
- [55] Z.-p. Li, H.-x. Ye, M.-h. Lu, An unified approach to pseudoscalar meson photoproductions off nucleons in the quark model, *Phys. Rev.* C56 (1997) 1099–1113. doi:10.1103/PhysRevC.56.1099.
- [56] M. Paris, Private communication (2010).
- [57] A. Matsuyama, T. Sato, T. S. H. Lee, Dynamical coupled-channel model of meson production reactions in the nucleon resonance region, *Phys. Rept.* 439 (2007) 193–253. doi:10.1016/j.physrep.2006.12.003.
- [58] A. Sarantsev, V. A. Nikonov, Private communication (2016).
- [59] I. Denisenko, A. V. Anisovich, V. Crede, H. Eberhardt, E. Klempt, V. A. Nikonov, A. V. Sarantsev, H. Schmieden, U. Thoma, A. Wilson,  $N^*$  decays to  $N\omega$  from new data on  $\gamma p \rightarrow \omega p$ , *Phys. Lett.* B755 (2016) 97–101. doi:10.1016/j.physletb.2016.01.061.